Article

Reconfiguration Analysis and Characteristics of a Novel 8-Link Variable-DOF Planar Mechanism with Five Motion Modes

Xianwen Kong [1,*] **and Jieyu Wang** [2]

[1] School of Engineering and Physical Sciences, Heriot-Watt University, Edinburgh EH14 4AS, UK
[2] School of Mechatronic Engineering and Automation, Shanghai University, Shanghai 200444, China; jywang2021@shu.edu.cn
[*] Correspondence: x.kong@hw.ac.uk

Abstract: Variable-DOF (or kinematotropic) mechanisms are a class of reconfigurable mechanisms that have varying degrees of freedom (DOF) in different motion modes and can be reconfigured without disassembly. However, the number of proposed variable-DOF multi-loop planar mechanisms is currently limited. This paper introduces a new 8-link variable-DOF planar mechanism that has five motion modes. Firstly, the 8-link variable-DOF planar mechanism is described. Then, reconfiguration analysis of the mechanism is performed using a hybrid approach that combines elimination and computer algebraic geometry methods. The analysis reveals that the 8-link mechanism has one 2-DOF motion mode and four 1-DOF motion modes. It can switch among three motion modes at four transition configurations and between two motion modes at the remaining four transition configurations. The paper also highlights the geometric characteristics of the mechanism in different motion modes. In contrast to variable-DOF planar mechanisms presented in the literature, the proposed 8-link mechanism has two inactive joints in one of its 1-DOF motion modes. Moreover, both closed-loop 4R kinematic sub-chains of the mechanism must appear as either a pair of parallelograms or a pair of anti-parallelograms in the same motion mode. As a by-product of this research, a method for factoring trigonometric functions in two angles is also proposed.

Keywords: variable-DOF mechanism; reconfigurable mechanism; reconfiguration analysis; motion mode; factorization of two-angle trigonometric function

1. Introduction

One of the current research focuses in mechanisms and robotics is reconfigurable mechanisms and robots [1,2], which could help meet the needs of robots and manufacturing systems that can rapidly adapt to changes in environment and production.

Variable-DOF (or kinematotropic) mechanisms [3–15] are a class of reconfigurable mechanisms that have varying degrees of freedom (DOF) in different motion modes and can be reconfigured without disassembly. Considerable progress has been made in the type synthesis and reconfiguration analysis of variable-DOF mechanisms, including single-loop spatial mechanisms [5,7,12], parallel mechanisms [11,13–20], multi-mode mobile parallel mechanisms [21], and multi-loop mechanisms [4,5,22–29]. It should be noted that variable-DOF mechanisms are composed of conventional kinematic joints and do not involve variable kinematic joints [30], reconfigurable kinematic joints [31] or metamorphic kinematic joints [32].

Apart from the construction methods [7,23,27], most approaches for the type synthesis of variable-DOF mechanisms are based on different mathematical methods ranging from displacement group theory [5,11], intersection of surfaces [10,20], factorization of polynomials [12,33], and primary decomposition of ideals [14,17–19] to the comprehensive Gröbner basis of parametric polynomial equations [19,34]. Through the construction methods in [7,23,27], a number of variable-DOF mechanisms have been constructed from

existing overconstrained mechanisms. No overconstrained mechanisms are required in advance if using methods in [5,10–12,33]; however, only several variable-DOF mechanisms have been obtained by using these methods. Using the methods in [14,17,18], one can detect whether a multi-DOF overconstrained parallel mechanism is a variable-DOF parallel mechanism. Using the methods in [19,34], one can investigate the impact of link parameters of multi-DOF overconstrained parallel mechanism on the number and types of motion modes and identify different variable-DOF parallel mechanisms of the same topological structure. Variable-DOF mechanisms were obtained by using multi-mode single-loop kinematic chains as building blocks in [16,23]. With further development and application of the above methods, more and more variable-DOF mechanisms are expected to be revealed.

Methods for the reconfiguration analysis of variable-DOF mechanisms mainly include the elimination approaches [22], algebraic geometry methods [24,35,36], numerical algebraic geometry methods [37], branch-and-prune methods [38], singular value decomposition approaches [39–42], and the higher-order kinematics based approaches [43–46]. The first five methods can be used to identify all the motion modes of a variable-DOF mechanism as long as the link parameters of the mechanism are given, whereas a singular or transition configuration of the variable-DOF mechanism must be given in advance if the last method, which is more computationally efficient, is used for the reconfiguration analysis.

It is noted that there are no variable-DOF planar single-loop mechanisms composed of R (revolute) and P (prismatic) joints, and the number of variable-DOF multi-loop planar mechanisms is still very limited. The only four variable-DOF multi-loop planar mechanisms proposed so far are the 12-link Wunderlich mechanism in [3], the 10-link Kovalev mechanism in [4], the 8-link variable-DOF planar mechanism in [5], and the 8-link variable-DOF planar mechanism in [47].

One difference between these four variable-DOF multi-loop planar mechanisms lies in the number of their inactive joints. An inactive joint in a variable-DOF mechanism under a specified motion mode is a kinematic joint that loses its DOF due to intrinsic constraints within the mechanism. The 8-link variable-DOF planar mechanism proposed in [5] has four inactive joints in its 3-DOF motion mode and no inactive joint in its 1-DOF motion mode. In the 3-DOF motion mode, this 8-link mechanism degenerates to a planar serial 3R mechanism. The 8-link variable-DOF planar mechanism presented in [47] has four inactive joints in four of its 1-DOF motion modes and no inactive joint in its 2-DOF motion mode. In these four 1-DOF motion modes, a closed-loop 4R kinematic sub-chain of the 8-link mechanism degenerates (or loses its DOF).

One question arising from the above observations is the following: Are there variable-DOF 8-link planar mechanisms which have neither a serial mechanism motion mode nor a motion mode with a degenerated closed-loop 4R sub-kinematic chain? This paper will answer the above question by presenting a novel 8-link variable-DOF planar mechanism. As will be shown later, this 8-link mechanism has two inactive joints in one of its 1-DOF motion modes and no inactive joints in the other motion modes.

This paper is organized as follows. In Section 2, a geometric description of a novel variable-DOF 8-link planar mechanism is given. A set of kinematic equations is set up in Section 3 with the variables selected to better reflect the geometric characteristics of the mechanism in different motion modes. The motion modes and transition configurations of the variable-DOF 8-link planar mechanism are identified using a hybrid approach that combines elimination and computer algebraic geometry methods in Sections 4 and 5. The reconfiguration of the variable-DOF 8-link planar mechanism is detailed in Section 6. Finally, conclusions are drawn.

2. Geometric Description of a Novel 8-Link Variable-Dof Planar Mechanism

The 8-link variable-DOF planar mechanism [47] constructed using two parallelograms is composed of four binary links and four triangular ternary links and has four inactive joints in four of its 1-DOF motion modes and no inactive joint in its 2-DOF motion mode. Recently, it was revealed in [48] that in addition to the 1-DOF motion mode, a 3-RR planar

parallelogram may have up to two structure modes if the two ternary links are triangular or no structure mode if the two ternary links are collinear. The four inactive joints in a motion mode of the 8-link variable-DOF planar mechanism correspond to the structure mode of a 3-RR planar parallelogram. Using two parallelograms with no structure mode, we can construct an 8-link variable-DOF planar mechanism that does not have 1-DOF motion mode with four inactive joints. Alternatively, by simply replacing each triangular ternary link in the 8-link variable-DOF planar mechanism in [47] with a collinear ternary link, the 1-DOF motion modes with four inactive joints of the original 8-link mechanism will be eliminated. This would lead to a novel 8-link variable-DOF planar mechanism (Figure 1).

The novel 8-link variable-DOF planar mechanism is composed of four identical binary links, $A_{11}B_{11}$, $A_{12}B_{12}$, $A_{21}B_{21}$, and $A_{22}B_{22}$, and four identical collinear ternary links, $AA_{11}A_{12}$, $BB_{11}B_{12}$, $AA_{21}A_{22}$, and $BB_{21}B_{22}$, connected by 10 R joints. Link $A_{22}B_{22}$ is the frame. The link parameters of the 8-link variable-DOF planar mechanism are

$AA_{11} = BB_{11} = AA_{21} = BB_{21} = a_1$, $AA_{12} = BB_{12} = AA_{22} = BB_{22} = a_2$, and $A_{11}B_{11} = A_{12}B_{12} = A_{21}B_{21} = A_{22}B_{22} = L_1$.

The link parameters of an example 8-link variable-DOF planar mechanism are $a_1 = 45$, $a_2 = 75$, and $L_1 = 25$. Here, link lengths are represented by dimensionless numbers that indicate their relative length, subject to the condition that $L_1 < (a_2 - a_1)$ in order to avoid link interference.
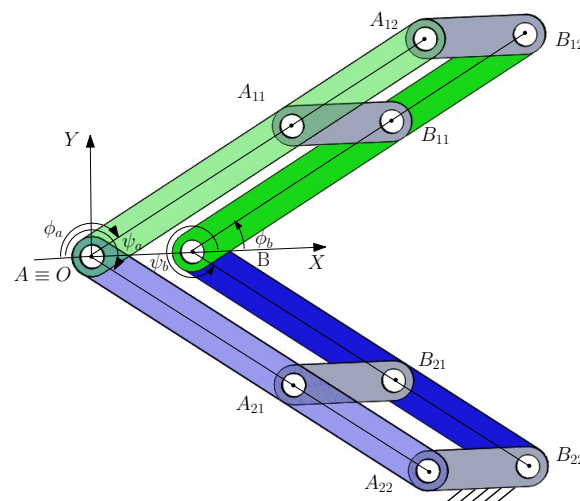

Figure 1. A novel 8-link variable-DOF planar mechanism.

3. Kinematic Equations

To facilitate the identification of the geometric characteristics of the 8-link mechanism, the coordinate system *O-XY* is set up such that *O* coincides with R joint center *A*, and R joint center *B* is located on the positive *X*-axis. Let ϕ_a (ψ_a) denote the angle between the negative direction of the *X*-axis and the link AA_{11} (AA_{21}) measured clockwise and ϕ_b (ψ_b) the angle between the positive direction of the *X*-axis and the link BB_{11} (BB_{21}) measured anti-clockwise. An auxiliary variable, $L = AB$ ($L > 0$), is introduced to simplify the reconfiguration analysis.

The loop closure equations of loops $ABB_{11}A_{11}A$, $ABB_{12}A_{12}A$, $ABB_{21}A_{21}A$, and $ABB_{22}A_{22}A$ written in vector form are

$$
\begin{cases}
(\overrightarrow{AB} + \overrightarrow{BB_{11}} - \overrightarrow{AA_{11}}) \cdot (\overrightarrow{AB} + \overrightarrow{BB_{11}} - \overrightarrow{AA_{11}}) = L_1^2 \\
(\overrightarrow{AB} + \overrightarrow{BB_{12}} - \overrightarrow{AA_{12}}) \cdot (\overrightarrow{AB} + \overrightarrow{BB_{12}} - \overrightarrow{AA_{12}}) = L_1^2 \\
(\overrightarrow{AB} + \overrightarrow{BB_{21}} - \overrightarrow{AA_{21}}) \cdot (\overrightarrow{AB} + \overrightarrow{BB_{21}} - \overrightarrow{AA_{21}}) = L_1^2 \\
(\overrightarrow{AB} + \overrightarrow{BB_{22}} - \overrightarrow{AA_{22}}) \cdot (\overrightarrow{AB} + \overrightarrow{BB_{22}} - \overrightarrow{AA_{22}}) = L_1^2
\end{cases}
$$

Rewriting the above equation in complex number form, we have

$$
\begin{cases}
(L + a_1 e^{i\phi_b} - a_1 e^{i(\pi - \phi_a)})(L + a_1 e^{-i\phi_b} - a_1 e^{-i(\pi - \phi_a)}) - L_1^2 = 0 \\
(L + a_2 e^{i\phi_b} - a_2 e^{i(\pi - \phi_a)})(L + a_2 e^{-i\phi_b} - a_2 e^{-i(\pi - \phi_a)}) - L_1^2 = 0 \\
(L + a_1 e^{i\psi_b} - a_1 e^{i(\pi - \psi_a)})(L + a_1 e^{-i\psi_b} - a_1 e^{-i(\pi - \psi_a)}) - L_1^2 = 0 \\
(L + a_2 e^{i\psi_b} - a_2 e^{i(\pi - \psi_a)})(L + a_2 e^{-i\psi_b} - a_2 e^{-i(\pi - \psi_a)}) - L_1^2 = 0
\end{cases}
$$

Simplifying the above equation, we obtain

$$
\begin{cases}
a_1 C(\phi_b + \phi_a) + L(C\phi_b + C\phi_a) + (L^2 - L_1^2)/(2a_1) + a_1 = 0 \\
a_2 C(\phi_b + \phi_a) + L(C\phi_b + C\phi_a) + (L^2 - L_1^2)/(2a_2) + a_2 = 0 \\
a_1 C(\psi_b + \psi_a) + L(C\psi_b + C\psi_a) + (L^2 - L_1^2)/(2a_1) + a_1 = 0 \\
a_2 C(\psi_b + \psi_a) + L(C\psi_b + C\psi_a) + (L^2 - L_1^2)/(2a_2) + a_2 = 0
\end{cases}
\tag{1}
$$

where $S*$ and $C*$ denote $\sin *$ and $\cos *$, respectively.

4. Motion Mode Analysis of an 8-Link Variable-Dof Planar Mechanism Using a Hybrid Approach

In this section, we will reveal all the motion modes of the novel 8-link variable-DOF mechanism (Figure 1) by using resultant elimination, which has been extensively used in the kinematic analysis of mechanisms [49,50], and the primary decomposition of ideals from computer algebraic geometry [35], which has been used in the reconfiguration analysis of multi-mode mechanisms [17,24,36].

Eliminating ϕ_b from the first and second equations of Equation (1) and ψ_b from the third and fourth equations of Equation (1), Equation (1) is reduced to the following set of two equations in three variables ϕ_a, ψ_a, and L (see Appendix A for details)

$$
\begin{cases}
(1 - C^2\phi_a)[1 - (k_2 - C\phi_a)^2] - [k_1 - C\phi_a(k_2 - C\phi_a)]^2 = 0 \\
(1 - C^2\psi_a)[1 - (k_2 - C\psi_a)^2] - [k_1 - C\psi_a(k_2 - C\psi_a)]^2 = 0
\end{cases}
\tag{2}
$$

where $k_1 = (L^2 - L_1{}^2)/(2a_1 a_2) - 1$ and $k_2 = -(a_1 + a_2)(L^2 - L_1{}^2)/(2La_1 a_2)$.

For simplicity reasons and without loss of generality, we will investigate the reconfiguration analysis of the 8-link variable-DOF mechanism via the example mechanism given in Section 2. Substituting the link parameters of the example 8-link mechanism into Equation (2), we obtain

$$
\begin{cases}
(L - 25)(L + 25)f_1 = 0 \\
(L - 25)(L + 25)f_2 = 0
\end{cases}
\tag{3}
$$

where $f_1 = L^4 + 240L^3 C\phi_a + 6750C(2\phi_a)L^2 + 7025L^2 - 150,000C\phi_a L - 9,000,000$ and $f_2 = L^4 + 240L^3 C\psi_a + 6750C(2\psi_a)L^2 + 7025L^2 - 150,000C\psi_a L - 9,000,000$.

Since $L > 0$, Equation (3) leads to two cases:

Case A

$$
L - 25 = 0
\tag{4}
$$

Equation (4) represents a 2-DOF motion mode, motion mode 1 (Figure 2a), of the 8-link mechanism. In motion mode 1, both closed-loop 4R kinematic sub-chains, $A_{11}B_{11}B_{12}A_{12}$ and $A_{21}B_{21}B_{22}A_{22}$, are parallelograms. Throughout the remainder of this paper, including Figure 2, line AB will be kept in a horizontal position by releasing the frame. This is to ensure that the geometric characteristics of the 8-link mechanism are clearly illustrated.
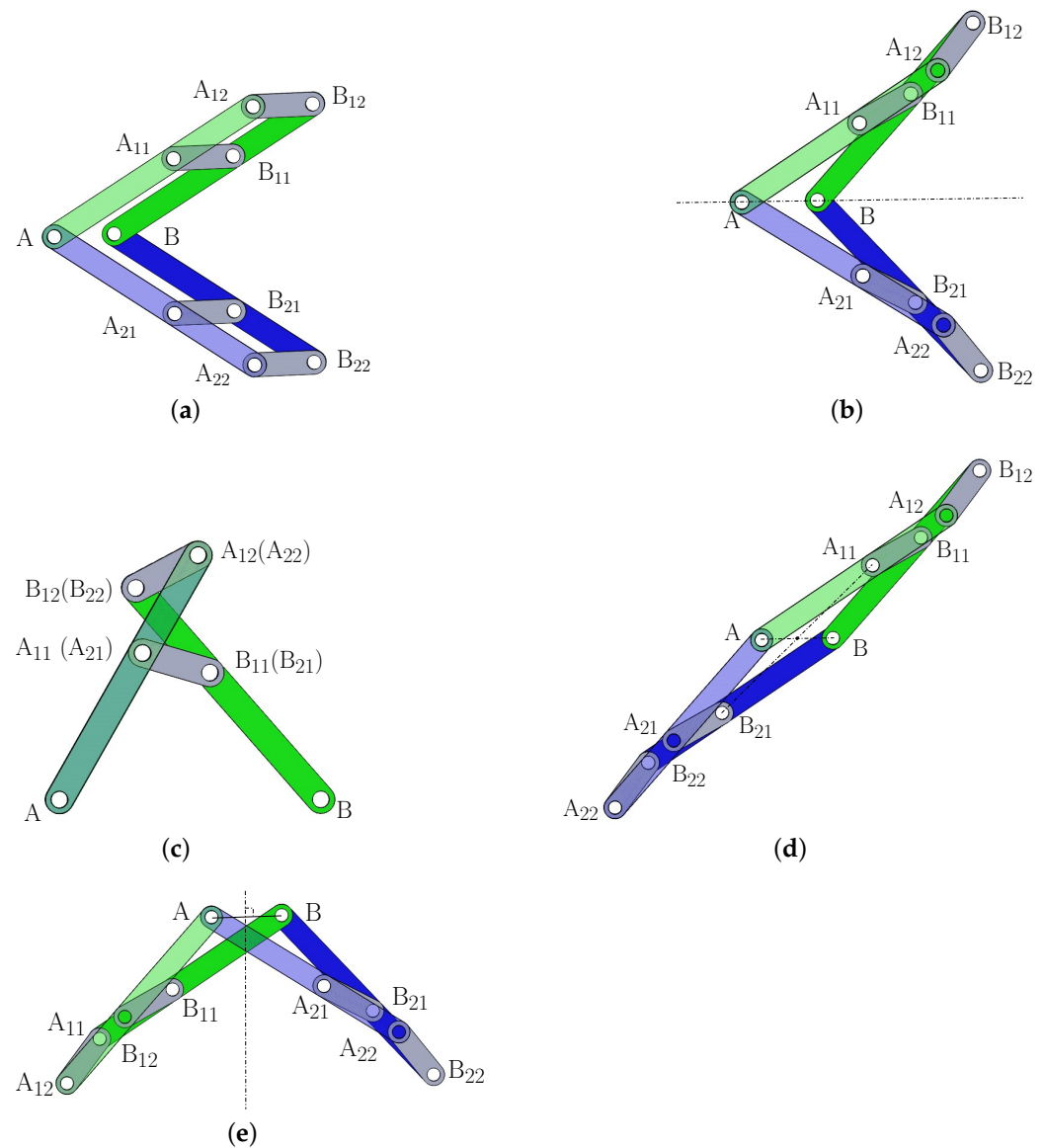
Figure 2. The 8-link variable-DOF planar mechanism in (**a**) 2-DOF motion mode 1; (**b**) 1-DOF motion mode 2: Kite motion mode; (**c**) 1-DOF motion mode 3: Planar 4R mechanism mode; (**d**) 1-DOF motion mode 4: Parallelogram motion mode; and (**e**) 1-DOF motion mode 5: Isosceles trapezium motion mode.

Case B

$$
\begin{cases}
L^4 + 240L^3 C\phi_a + 6750 C(2\phi_a)L^2 + 7025L^2 - 150,000C\phi_a L - 9,000,000 = 0 \\
L^4 + 240L^3 C\psi_a + 6750 C(2\psi_a)L^2 + 7025L^2 - 150,000C\psi_a L - 9,000,000 = 0
\end{cases}
\tag{5}
$$

In the following, we will identify the motion modes associated with Equation (5) by eliminating *L* using resultant first and then using the primary decomposition of ideals from the algebraic geometry [35] to find the positive-dimensional solutions to the resulted equations.

Eliminating *L* using resultants from Equation (5), we obtain

$$
36,905,625,000,000,000,000,000,000g(C\phi_a - C\psi_a)^4 = 0
\tag{6}
$$

where $g = 72,900C\phi_a^4 - 5940C\phi_a^3 C\psi_a - 215,280C\phi_a^2 C\psi_a^2 - 5940C\phi_a C\psi_a^3 + 72,900C\psi_a^4 + 63,661C\phi_a^2 + 12,122C\phi_a C\psi_a + 63,661C\psi_a^2 - 57,600.$

From Equation (6), we obtain the following two sub-cases

$$C\phi_a - C\psi_a = 0 \tag{7}$$

and

$$g = 0 \tag{8}$$

Equation (7) has two solutions:

$$\psi_a = -\phi_a \tag{9}$$

and

$$\psi_a = \phi_a \tag{10}$$

Equation (9) represents a 1-DOF motion mode, motion mode 2 (Figure 2b), of the 8-link mechanism. In motion mode 2, both closed-loop 4R sub-kinematic chains, $A_{11}B_{11}B_{12}A_{12}$ and $A_{21}B_{21}B_{22}A_{22}$, are anti-parallelograms, and the 8-link mechanism is symmetric about line AB. Motion mode 2 is called the kite motion mode because, in this motion mode, the 8-link mechanism takes the shape of a kite.

Equation (10) represents a 1-DOF motion mode, motion mode 3 (Figure 2c), of the 8-link mechanism. In motion mode 3, both closed-loop 4R kinematic sub-chains, $A_{11}B_{11}B_{12}A_{12}$ and $A_{21}B_{21}B_{22}A_{22}$, coincide, and the 8-link mechanism has two inactive joints A and B. Motion mode 3 is called the planar 4R mechanism mode because, in this motion mode, the 8-link mechanism degenerates to a planar 4R mechanism.

Using the primary decomposition of ideals from computer algebraic geometry, Equation (8) can be rewritten as (See Appendix B for details)

$$g_1 g_2 = 0 \tag{11}$$

where $g_1 = -281 + 135C(2\phi_a) - 306C(\phi_a - \psi_a) + 295C(\phi_a + \psi_a) + 135C(2\psi_a)$ and $g_2 = -281 + 135C(2\phi_a) + 295C(\phi_a - \psi_a) - 306C(\phi_a + \psi_a) + 135C(2\psi_a)$.

Equation (11) has two solutions:

$$g_1 = 0 \tag{12}$$

and

$$g_2 = 0 \tag{13}$$

Equation (12) represents a 1-DOF motion mode, motion mode 4 (Figure 2d), of the 8-link mechanism. In motion mode 4, both closed-loop 4R sub-kinematic chains, $A_{11}B_{11}B_{12}A_{12}$ and $A_{21}B_{21}B_{22}A_{22}$, are anti-parallelograms, and the 8-link mechanism is rotational symmetric. Motion mode 4 is called the parallelogram motion mode because, in this motion mode, the 8-link mechanism is in the shape of a parallelogram.

Equation (13) represents a 1-DOF motion mode, motion mode 5 (Figure 2e), of the 8-link mechanism. In motion mode 5, both closed-loop 4R kinematic sub-chains, $A_{11}B_{11}B_{12}A_{12}$ and $A_{21}B_{21}B_{22}A_{22}$, are anti-parallelograms, and the 8-link mechanism is symmetric about the perpendicular bisector of AB. Motion mode 5 is called the isosceles trapezium motion mode because, in this motion mode, the 8-link mechanism is in the shape of an isosceles trapezium.

It can be observed that if $(\phi_a^*, \psi_a^*, L^*)$ is a set of solution to Equation (5), then $(\pi \pm \phi_a^*, \pi \pm \psi_a^*, -L^*)$ are also solutions to Equation (5). Since $L > 0$, the $\phi_a - \psi_a$ curve for motion mode 4 (or 5) (see Figure 3) is only one half of the curve obtained using Equation (12) (or Equation (13)) that lies outside of the region enclosed by lines $\psi_a - \phi_a = \pm\pi$ (or

$\phi_a + \psi_a = \pm \pi$). In other words, in motion mode 4, we have $\psi_a - \phi_a > \pi$ or $\psi_a - \phi_a < -\pi$. In motion mode 5, we have $\psi_a + \phi_a > \pi$ or $\psi_a + \phi_a < -\pi$.
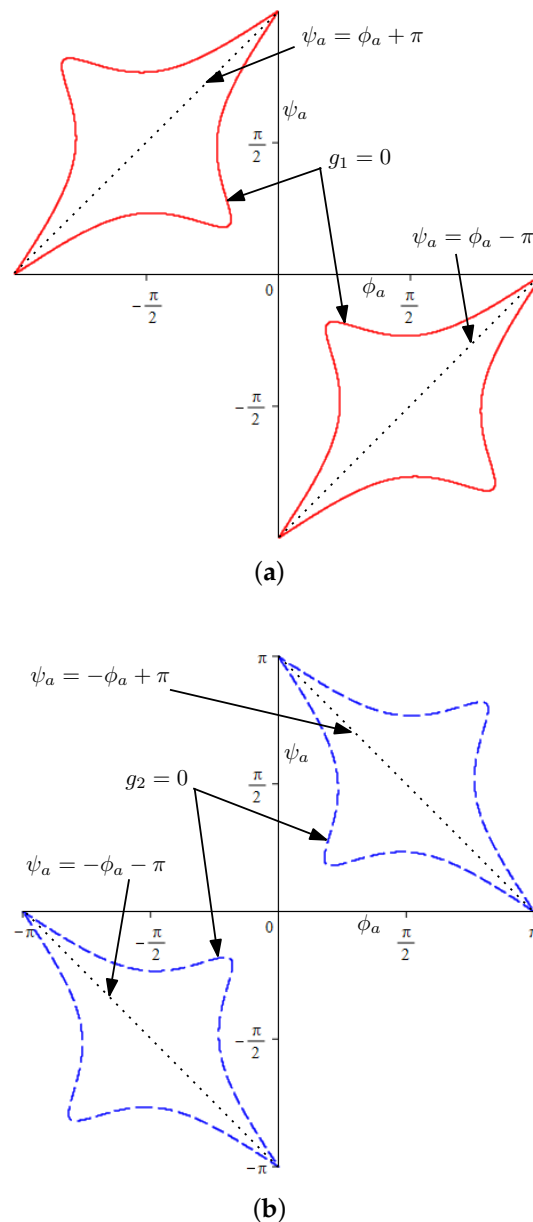

(a)

(b)

Figure 3. Kinematic analysis of the 8-link variable-DOF planar mechanism in: (**a**) motion mode 4; (**b**) motion mode 5.

In summary, the 8-link variable-DOF mechanism has one 2-DOF motion mode and four 1-DOF motion modes (Figure 2). Table 1 summarizes all the five motion modes of the 8-link mechanism and their geometric characteristics. Figure 4 shows the $\phi_a - \psi_a$ curves for the four 1-DOF motion modes 2 (Equation (9)), 3 (Equation (10)), 4 (Equation (12)) and 5 (Equation (13)).

Unlike the two 8-link variable-DOF planar mechanisms in [5,47] which have four inactive joints in some of their motion modes, this 8-link variable-DOF planar mechanism has two inactive joints A and B in one of the 1-DOF motion modes (motion mode 3).

Figure 2 shows that both closed-loop 4R kinematic sub-chains of this novel 8-link variable-DOF planar mechanism must appear as parallelograms in its 2-DOF motion mode or anti-parallelograms in any of its 1-DOF motion mode, whereas both the 8-link variable-

DOF planar mechanism [47] and the 12-link Wunderlich mechanism have a motion mode with an odd number of 4R sub-kinematic chains appearing as anti-parallelograms.

Table 1. Five motion modes of the 8-link variable-DOF mechanism.

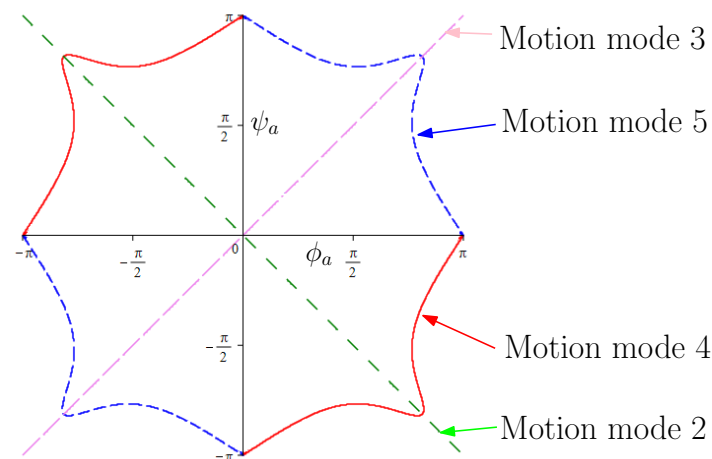| No	DOF	Constraint Equations	Description
1	2	$L = 25$	Both closed-loop 4R sub-kinematic chains are parallelograms (Figure 2a). ϕ_a and ψ_a are independent.
2	1	$\psi_a = -\phi_a$	Both closed-loop 4R kinematic sub-chains are anti-parallelograms. The 8-link mechanism is symmetric about line AB (Figure 2b).
3	1	$\psi_a = \phi_a$	Both closed-loop 4R sub-kinematic chains are anti-parallelograms that coincide with each other (Figure 2c), and the 8-link mechanism has two inactive joints A and B.
4	1	$\begin{aligned} &-281 + 135C(2\phi_a) \\ &-306C(\phi_a - \psi_a) \\ &+295C(\phi_a + \psi_a) \\ &+135C(2\psi_a) = 0 \end{aligned}$	Both closed-loop 4R kinematic sub-chains are anti-parallelograms. The 8-link mechanism is rotational symmetric (Figure 2d).
5	1	$\begin{aligned} &-281 + 135C(2\phi_a) \\ &+295C(\phi_a - \psi_a) \\ &-306C(\phi_a + \psi_a) \\ &+135C(2\psi_a) = 0 \end{aligned}$	Two closed-loop 4R sub-kinematic chains are anti-parallelograms. The 8-link mechanism is symmetric about the perpendicular bisector of AB (Figure 2e).

Figure 4. Four 1-DOF motion modes on $\phi_a - \psi_a$ plane.

Although one can solve Equation (5) directly using the primary decomposition of ideals to identify all the motion modes of the 8-link variable-DOF mechanism, it was found hard to obtain the concise equations (Equations (12) and (13)) for motion modes 4 and 5 that were obtained by eliminating L before calculating the primary decomposition of ideals.

It is important to note that the reconfiguration analysis approach described in [47] is not applicable to the 8-link variable-DOF planar mechanism shown in Figure 1. This is because the method in [47] cannot distinguish between motion mode 2 (Figure 2b) and motion mode 4 (Figure 2d), or between motion mode 3 (Figure 2c) and motion mode 5 (Figure 2e), for this mechanism.

5. Transition Configuration Analysis of the 8-Link Variable-Dof Planar Mechanism

The transition configurations between two or more motion modes can be obtained by solving the kinematic equations composed of equations of these motion modes [36].

Let us take the transition configurations between motion modes 2 and 4, T(2 ∧ 4), of the 8-link mechanism as an example.

The set of equations composed of Equations (9) (motion mode 2) and (12) (motion mode 4) is

$$\begin{cases} \psi_a = -\phi_a \\ -281 + 135C(2\phi_a) - 306C(\phi_a - \psi_a) + 295C(\phi_a + \psi_a) + 135C(2\psi_a) = 0 \end{cases} \tag{14}$$

Section 4 shows that in motion mode 4, we have $\psi_a - \phi_a > \pi$ or $\psi_a - \phi_a < -\pi$. Solving Equation (14) under these conditions, we obtain two solutions:

$$\begin{cases} \phi_a = 2.5559(rad) \\ \psi_a = -\phi_a \end{cases} \tag{15}$$

$$\begin{cases} \phi_a = -2.5559(rad) \\ \psi_a = -\phi_a \end{cases} \tag{16}$$

Equations (15) and (16) show that there are two transition configurations between motion modes 2 and 4, T(2 ∧ 4)$_I$ (Figure 5a) and T(2 ∧ 4)$_{II}$ (Figure 5b). In these two transition configurations, links $A_{i1}B_{i1}$ and $B_{i2}A_{i2}$ are parallel to AB. One can readily obtain that the instantaneous DOF of the 8-link variable-DOF mechanism is two in these transition configurations. The details are omitted here since the calculation of instantaneous DOF of a mechanism has been well-documented in the literature.
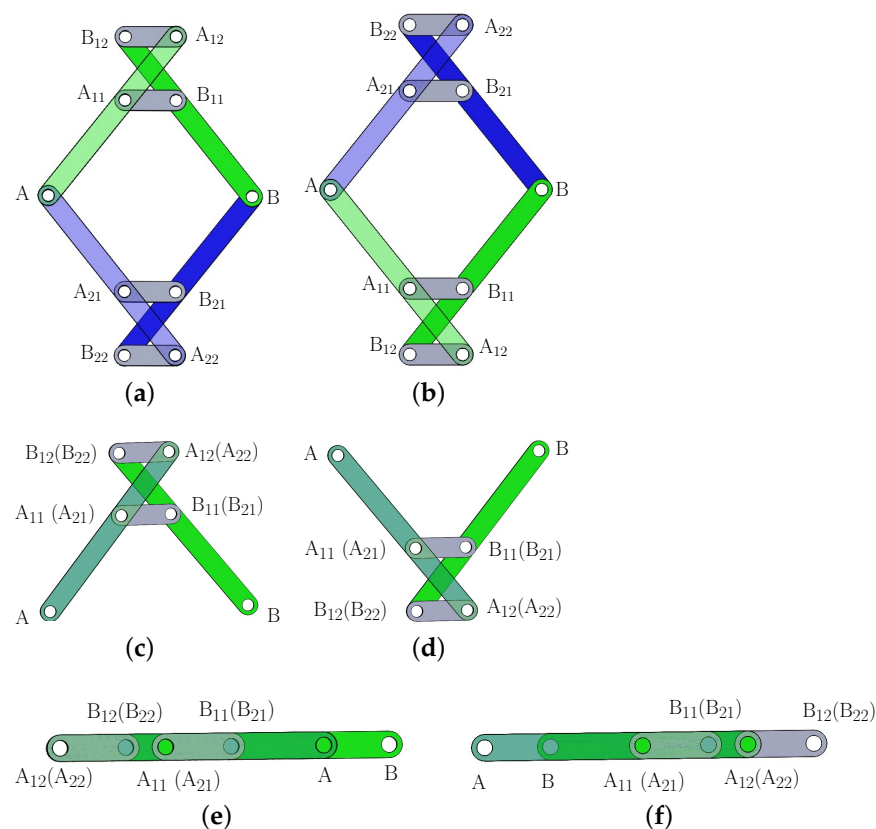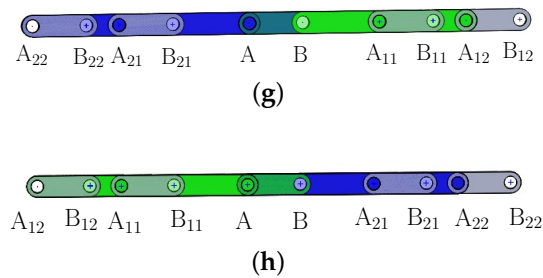

Figure 5. *Cont.*

A_{22} B_{22} A_{21} B_{21} A   B A_{11} B_{11} A_{12} B_{12}

(g)

A_{12} B_{12} A_{11} B_{11} A   B A_{21} B_{21} A_{22} B_{22}

(h)

Figure 5. The 8-link variable-DOF planar mechanism in transition configuration: (**a**) $T(2 \wedge 4)_I$; (**b**) $T(2 \wedge 4)_{II}$; (**c**) $T(3 \wedge 5)_I$; (**d**) $T(3 \wedge 5)_{II}$; (**e**) $T(1 \wedge 2 \wedge 3)_I$; (**f**) $T(1 \wedge 2 \wedge 3)_{II}$; (**g**) $T(1 \wedge 4 \wedge 5)_I$; and (**h**) $T(1 \wedge 4 \wedge 5)_{II}$.

Following the above steps, we can identify six more transition configurations of the 8-link mechanism, including two transition configurations, $T(3 \wedge 5)_I$ (Figure 5c) and $T(3 \wedge 5)_{II}$) (Figure 5d), in which the mechanism can switch between two motion modes and four transition configurations, ($T(1 \wedge 2 \wedge 3)_I$ (Figure 5e), $T(1 \wedge 2 \wedge 3)_{II}$ (Figure 5f), $T(1 \wedge 4 \wedge 5)_I$ (Figure 5g), and $T(1 \wedge 4 \wedge 5)_{II}$) (Figure 5h), in which the mechanism can switch among three motion modes. It is noted that there are no transition configurations between motion modes 2 and 5 or between motion modes 3 and 4. The geometric characteristics of the 8-link mechanism in all the eight transition configurations are summarized in Table 2. All the transition configurations are singular configurations. The instantaneous DOF of the 8-link variable-DOF in transition configurations can be readily obtained as two in transition configurations $T(2 \wedge 4)_I$, $T(2 \wedge 4)_{II}$, $T(3 \wedge 5)_I$, and $T(3 \wedge 5)_{II}$ and four in transition configurations $T(1 \wedge 2 \wedge 3)_I$, $T(1 \wedge 2 \wedge 3)_{II}$, $T(1 \wedge 4 \wedge 5)_I$, and $T(1 \wedge 4 \wedge 5)_{II}$.

Table 2. Transition configurations of the 8-link mechanism.

No	ϕ_a and ψ_a (rad)	Description	Instantaneous DOF
$T(2 \wedge 4)_I$	$\begin{cases} \phi_a = 2.5559 \\ \psi_a = -\phi_a \end{cases}$	Links $A_{i1}B_{i1}$ and $B_{i2}A_{i2}$ are parallel to AB (Figure 5a).	2
$T(2 \wedge 4)_{II}$	$\begin{cases} \phi_a = -2.5559 \\ \psi_a = -\phi_a \end{cases}$	Links $A_{i1}B_{i1}$ and $B_{i2}A_{i2}$ are parallel to AB (Figure 5b).	
$T(3 \wedge 5)_I$	$\begin{cases} \phi_a = 2.5559 \\ \psi_a = \phi_a \end{cases}$	Links $A_{i1}B_{i1}$ and $B_{i2}A_{i2}$ (i = 1 and 2) are parallel to AB (Figure 5c).	
$T(3 \wedge 5)_{II}$	$\begin{cases} \phi_a = -2.5559 \\ \psi_a = \phi_a \end{cases}$	Links $A_{i1}B_{i1}$ and $B_{i2}A_{i2}$ (i = 1 and 2) are parallel to AB (Figure 5d).	
$T(1 \wedge 2 \wedge 3)_I$	$\begin{cases} \phi_a = 0 \\ \psi_a = 0 \end{cases}$	All the R joint centers are collinear (Figure 5e).	4
$T(1 \wedge 2 \wedge 3)_{II}$	$\begin{cases} \phi_a = \pi \\ \psi_a = \pi \end{cases}$	All the R joint centers are collinear (Figure 5f).	
$T(1 \wedge 4 \wedge 5)_I$	$\begin{cases} \phi_a = \pi \\ \psi_a = 0 \end{cases}$	All the R joint centers are collinear (Figure 5g).	
$T(1 \wedge 4 \wedge 5)_{II}$	$\begin{cases} \phi_a = 0 \\ \psi_a = \pi \end{cases}$	All the R joint centers are collinear (Figure 5h).	

6. Reconfiguration of the Variable-Dof 8-Link Planar Mechanism

Figure 6 illustrates the reconfiguration of the 8-link planar mechanism among the five motion modes via the eight transition configurations in the $\phi_a - \psi_a$ plane. The curves in the $\phi_a - \psi_a$ plane of the four 1-DOF motion modes, motion modes 2, 3, 4, and 5, are shown in green, pink, red, and blue, respectively. The 2-DOF motion mode, motion mode 1 in which $L = 25$, covers the whole $\phi_a - \psi_a$ plane. However, the 8-link mechanism can only transit among motion modes 1, 2, and 3 at two transition configurations $T(1 \wedge 2 \wedge 3)_I$ and $T(1 \wedge 2 \wedge 3)_{II}$ and among motion modes 1, 4, and 5 at two transition configurations $T(1 \wedge 4 \wedge 5)_I$ and $T(1 \wedge 4 \wedge 5)_{II}$ since we have $L > 25$ in the other configurations in motion modes 2, 3, 4, and 5.

Photos of the LEGO model of this 8-link mechanism at all the transition configurations, configurations with $\phi_a = \pm\pi/2$ and/or $\psi_a = \pm\pi/2$ in 1-DOF motion modes 2, 3, 4, and 5, and a configuration with $\phi_a = \pi/2$ and $\psi_a = -\pi/2$ in 2-DOF motion mode 1 are given. To distinguish the only 2-DOF motion mode from the 1-DOF motion modes, the photos of the sample configuration and the four transition configurations associated with motion mode 1 are framed. In the LEGO model, the links are allocated in six layers, and the axis of R joint A is in a curved shape to allow the mechanism to switch among all the five motion modes through the eight transition configurations without link interference. An animation of the reconfiguration of the 8-link mechanism among the five motion modes can be found in the supplementary materials. In the animation, link $AA_{21}A_{22}$ is selected as the frame of the mechanism, and all "$\wedge$" have been omitted in the notations for transition configurations for simplicity reasons.
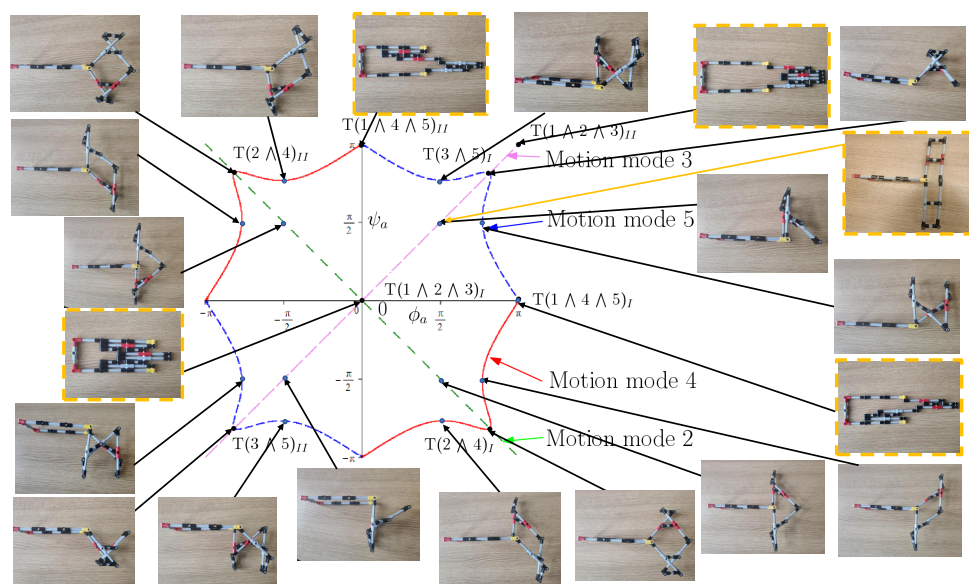

Figure 6. Reconfiguration of the example variable-DOF 8-link planar mechanism among the five motion modes.

The mechanism could be more compact if it is only required to switch among some but not all of its motion modes. For example, if one needs the 8-link mechanism to switch among four motion modes 1, 2, 4 and 5 only (Figure 7), all the links can be located in four layers without encountering link interference as shown in the CAD model of the mechanism in transition configuration $T(1 \wedge 4 \wedge 5)_I$. This four-layer 8-link planar mechanism could be used as a construction unit of new variable-DOF multi-loop mechanisms, which would enrich the types of reconfigurable/multi-mode deployable mechanisms [25–27,42,51,52].
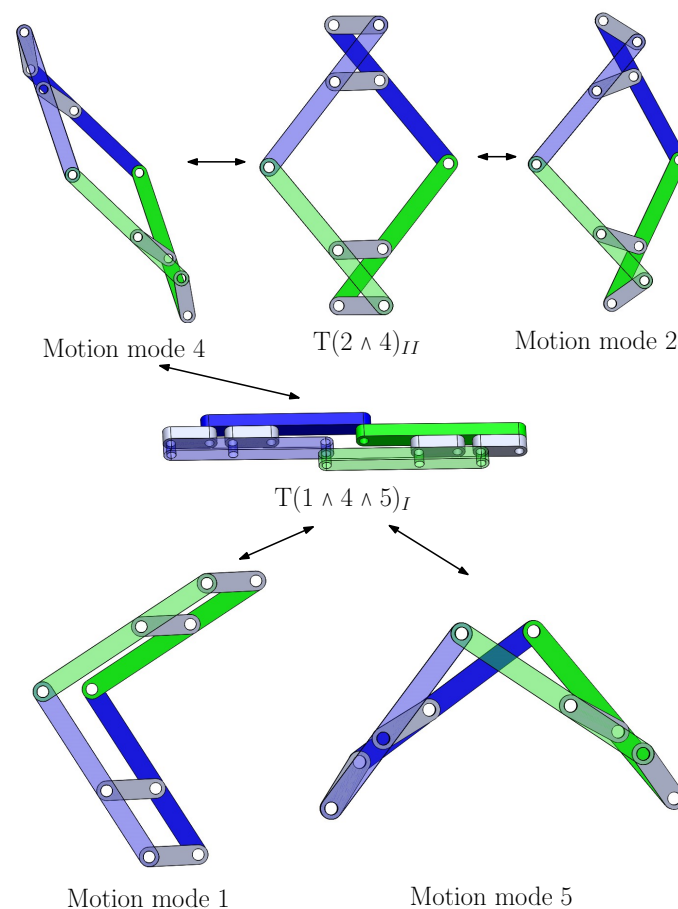
Figure 7. A variable-DOF 8-link planar mechanism in compact design that can transit among four motion modes.

7. Conclusions

A novel 8-link variable-DOF planar mechanism with five motion modes has been proposed. Reconfiguration analysis has shown that the mechanism has one 2-DOF double parallelogram motion mode and four 1-DOF motion modes. In addition, the mechanism can switch among three motion modes at four transition configurations and between two motion modes at four other transition configurations.

In contrast to the two 8-link variable-DOF planar mechanisms in [5,47], which have four inactive joints in some of their motion modes, this novel 8-link variable-DOF planar mechanism has two inactive joints in one of its 1-DOF motion modes. The two closed-loop 4R kinematic sub-chains of the novel mechanism must appear either as a pair of parallelograms in the 2-DOF motion mode or a pair of anti-parallelograms in a 1-DOF motion mode.

The hybrid approach that combines elimination and computer algebraic geometry methods has been found to be more efficient than the algebraic geometry approach without elimination. As a by-product, a method for factoring trigonometric functions in two angles has been proposed.

This work, together with reference [47], provides a starting point for the design and analysis of variable-DOF multi-loop mechanisms constructed using more than two parallelograms, which could be used as reconfigurable/multi-mode deployable mechanisms.

Appendix A. Derivation of Equation (2)

Solving the set of equations composed of the first and second equations in Equation (1) as a set of linear equations in $C(\phi_b + \phi_a)$ and $C\phi_b + C\phi_a$, we have

$$\begin{cases} C(\phi_a + \phi_b) = k_1 \\ C\phi_a + C\phi_b = k_2 \end{cases} \tag{A1}$$

To eliminate ϕ_b from Equation (A1), rewrite the first equation in Equation (A1) as

$$-S\phi_a S\phi_b = k_1 - C\phi_a C\phi_b$$

Squaring both sides, we have

$$(-S\phi_a S\phi_b)^2 = (k_1 - C\phi_a C\phi_b)^2$$

Eliminating $S\phi_a$ and $S\phi_b$ from the above equation using the trigonometric identities $S^2\phi_a + C^2\phi_a = 1$ and $S^2\phi_b + C^2\phi_b = 1$, we have

$$(1 - C^2\phi_a)(1 - C^2\phi_b) - (k_1 - C\phi_a C\phi_b)^2 = 0 \tag{A2}$$

Solving the second equation in Equation (A1) for $C\phi_b$, we obtain

$$C\phi_b = k_2 - C\phi_a \tag{A3}$$

Substituting Equation (A3) into Equation (A2), we obtain the following equation in L and ϕ_a.

$$(1 - C^2\phi_a)[1 - (k_2 - C\phi_a)^2] - [k_1 - C\phi_a(k_2 - C\phi_a)]^2 = 0 \tag{A4}$$

Similarly, the third and fourth equations in Equation (1) can be reduced to

$$(1 - C^2\psi_a)[1 - (k_2 - C\psi_a)^2] - [k_1 - C\psi_a(k_2 - C\psi_a)]^2 = 0 \tag{A5}$$

Combining Equations (A4) and (A5), we obtain Equation (2).

Appendix B. Derivation of Equation (11)

Equation (11) can be derived from Equation (8) using the primary decomposition of ideals in the following five steps.

Step 1: Convert Equation (8) into a polynomial equation.

Substituting $C\phi_a = ca$ and $C\psi_a = cb$ into Equation (8), we obtain a polynomial equation in ca and cb.

$$f = 0 \tag{A6}$$

where $f = 72{,}900ca^4 - 5940ca^3cb - 215{,}280ca^2cb^2 - 5940cacb^3 + 72{,}900cb^4 + 63{,}661ca^2 + 12{,}122cacb + 63{,}661cb^2 - 57{,}600$.

Step 2: Calculate the primary decomposition of ideal $\mathcal{J} =< f, ca^2 + sa^2 - 1, cb^2 + sb^2 - 1 >$, where $sa = S\phi_a$ and $sb = S\psi_a$. The last two polynomials correspond to the trigonometric identities $S^2\phi_a + C^2\phi_a = 1$ and $S^2\psi_a + C^2\psi_a = 1$.

Calculating the primary decomposition of $\mathcal{J}$ using computer algebra system software, such as MAPLE command *PrimeDecomposition(J, 'removeredundant')*, we have

$$\mathcal{J} = \bigcap_{j=1}^{2} \mathcal{J}_j \tag{A7}$$

where the irreducible components, $\mathcal{J}_1$ and $\mathcal{J}_2$, of $\mathcal{J}$ are
$\mathcal{J}_1 =< ca^2 + sa^2 - 1, \ cb^2 + sb^2 - 1, \ -270ca^2 + 11cacb - 270cb^2 + 601sasb + 551, 270ca^2sa + 601ca^2sb - 11cacbsa + 270cb^2sa - 551sa - 601sb, \ -162{,}270ca^2sa - 288{,}301ca^2sb + 6611cacbsa - 2970cacbsb + 72{,}900cb^2sb + 168{,}881sa + 212{,}431sb, 72{,}900ca^4 - 5940ca^3cb - 215{,}280ca^2cb^2 - 5940cacb^3 + 72{,}900cb^4 + 63{,}661ca^2 + 12{,}122cacb + 63{,}661cb^2 - 576{,}00>$, and $\mathcal{J}_2 =< ca^2 + sa^2 - 1, \ cb^2 + sb^2 - 1, \ 270ca^2 - 11cacb + 270cb^2 + 601sasb - 551, \ 270ca^2sa - 601ca^2sb - 11cacbsa + 270cb^2sa - 551sa + 601sb, \ 162{,}270ca^2sa - 288{,}301ca^2sb - 6611cacbsa - 2970cacbsb + 72{,}900cb^2sb - 168{,}881sa + 212{,}431sb, 72{,}900ca^4 - 5940ca^3cb - 215{,}280ca^2cb^2 - 5940cacb^3 + 72{,}900cb^4 + 63{,}661ca^2 + 12{,}122cacb + 63{,}661cb^2 - 57{,}600>$.

Step 3: Calculate the Gröbner basis for each irreducible component.

Using the MAPLE command, *Basis(J₁, tdeg(sa, ca, sb, cb))*, we obtain the Gröbner basis of $\mathcal{J}_1$ as
$\mathcal{J}'_1 =< cb^2 + sb^2 - 1, 270ca^2 - 11cacb + 270cb^2 - 601sasb - 551, 11cacb - 270cb^2 + 270sa^2 + 601sasb + 281 >$.

Similarly, the Gröbner basis of $\mathcal{J}_2$ is
$\mathcal{J}'_2 =< cb^2 + sb^2 - 1, 270ca^2 - 11cacb + 270cb^2 + 601sasb - 551, 11cacb - 270cb^2 + 270sa^2 - 601sasb + 281 >$.

Step 4: Convert the polynomials in each of the irreducible components into trigonometrical functions.

Substituting $ca = C\phi_a, sa = S\phi_a, cb = C\psi_a$ and $sb = S\psi_a$ into $\mathcal{J}'_1$ and simplifying the results, we obtain
$\mathcal{J}'_1 =< C^2\psi_a + S^2\psi_a - 1, 270C^2\phi_a - 11C\phi_aC\psi_a + 270C^2\psi_a + 601S\phi_aS\psi_a - 551, 11C\phi_aC\psi_a - 270C^2\psi_a + 270S^2\phi_a - 601S\phi_aS\psi_a + 281 >$. i.e., $\mathcal{J}'_1 =< 0, g_1, -g_1 >$
where $g_1 = -281 + 135C(2\phi_a) + 295C(\phi_a + \psi_a) - 306C(\phi_a - \psi_a) + 135C(2\psi_a)$.

Similarly, we obtain $\mathcal{J}'_2 =< 0, g_2, -g_2 >$
where $g_2 = -281 + 135C(2\phi_a) + 295C(\phi_a - \psi_a) - 306C(\phi_a + \psi_a) + 135C(2\psi_a)$.

Step 5: Divide the trigonometrical function in Equation (8) by the product of the trigonometrical functions obtained in Step 4.

Divide g by g_1g_2, we can readily obtain

$$g/(g_1g_2) = 1$$

i.e.

$$g = g_1g_2 \tag{A8}$$

Substituting Equation (A8) into Equation (8), we obtain Equation (11).

References

1. Xi, F.; Dai, J.S.; Ding, X.; van der Wijk, V. *Proceedings of the 5-th IEEE/IFToMM International Conference on Reconfigurable Mechanisms and Robots, Toronto, ON, Canada, 12–14 August 2021*; Ryerson University: Toronto, ON, Canada, 2021.
2. Herder, J.; van der Wijk, V. *Proceedings of the 2018 International Conference on Reconfigurable Mechanisms and Robots (ReMAR 2018)*; IEEE: Piscataway, NJ, USA, 2018.
3. Wohlhart, K. Kinematotropic linkages. In *Recent Advances in Robot Kinematics*; Lenarčič, J., Parenti-Castelli, V., Eds.; Kluwer Academic: Dordrecht, The Netherlands, 1996; pp. 359–368.
4. Kovalev, M.D. Geometric theory of hinge devices. *Russian Acad. Sci. Izv. Math.* **1995**, *44*, 43–68.
5. Galletti, C.; Fanghella, P. Single-loop kinematotropic mechanisms. *Mech. Mach. Theory* **2001**, *36*, 743–761. [CrossRef]
6. Díez-Martínez, C.R. Mobility and Connectivity in Spatial Kinematic Chains. Master's Thesis, Technological Institute of Celaya, Celaya, Mexico, 2005. (In Spanish)
7. Kong, X.; Pfurner, M. Type synthesis and reconfiguration analysis of a class of variable-DOF single-loop mechanisms. *Mech. Mach. Theory* **2015**, *85*, 116–128. [CrossRef]
8. López-Custodio, P.C.; Dai, J.S. Design of a variable-mobility linkage using the Bohemian dome. *ASME J. Mech. Des.* **2019**, *141*, 092303. [CrossRef]
9. Feng, H.; Chen, Y.; Dai, J.S.; Gogu, G. Kinematic study of the general plane-symmetric Bricard linkage and its bifurcation variations. *Mech. Mach. Theory* **2017**, *116*, 89–104. [CrossRef]
10. Lopez-Custodio, P.C.; Rico, J.M.; Cervantes-Sánchez, J.J.; Perez-Soto, G.I. Reconfigurable mechanisms from the intersection of surfaces. *ASME J. Mech. Robot.* **2016**, *8*, 021029. [CrossRef]
11. Fanghella, P.; Galletti, C.; Giannotti, E. Parallel robots that change their group of motion. In *Advances in Robot Kinematics*; Lenarčič, J., Roth, B., Eds.; Springer: Dordrecht, The Netherlands, 2006; pp. 49–56.
12. Liu, K.; Yu, J.; Kong, X. Structure synthesis and reconfiguration analysis of variable-degree-of-freedom single-loop mechanisms with prismatic joints using dual quaternions. *ASME J. Mech. Robot.* **2022**, *14*, 021009. [CrossRef]
13. Kong, X. Type synthesis of variable degree-of-freedom parallel manipulators with both planar and 3T1R operation modes. In Proceedings of the ASME 2012 International Design Engineering Technical Conferences & Computers and Information in Engineering Conference, Chicago, IL, USA, 12–15 August 2012; DETC2012-70621.
14. Coste, M.; Demdah, K.M. Extra modes of operation and self motions in manipulators designed for Schoenflies motion. *ASME J. Mech. Robot.* **2015**, *7*, 041020. [CrossRef]
15. Zeng, Q.; Ehmann, K.F.; Cao, J. Design of general kinematotropic mechanisms. *Robot. Comput. Integr. Manuf.* **2016**, *38*, 67–81. [CrossRef]
16. Zhang, K.; Dai, J.S. Screw-system-variation enabled reconfiguration of the Bennett plano-spherical hybrid linkage and its evolved parallel mechanism. *ASME J. Mech. Des.* **2015**, *137*, 062303. [CrossRef]
17. Nurahmi, L.; Caro, S.; Wenger, P.; Schadlbauer, J.; Husty, M. Reconfiguration analysis of a 4-RUU parallel manipulator. *Mech. Mach. Theory* **2016**, *96*, 269–289. [CrossRef]
18. Nurahmi, L.; Putrayudanto, P.; Wei, G.; Agrawal, S.K. Geometric constraint-based reconfiguration and self-motions of a four-CRU parallel mechanism. *ASME J. Mech. Robot.* **2021**, *13*, 433748391. [CrossRef]
19. Kong, X. Classification of a 3-RER parallel manipulator based on the type and number of operation modes. *ASME J. Mech. Robot.* **2021**, *13*, 021013. [CrossRef]
20. López-Custodio, P.C.; Müller, A.; Dai, J.S. A kinematotropic parallel mechanism reconfiguring between three motion branches of different mobility. In *Advances in Mechanism and Machine Science. IFToMM WC 2019*; Uhl, T., Ed.; Springer: Cham, Switzerland, 2019; pp. 2611–2620.
21. Liu, Y.; Li, Y.; Yao, Y.-A.; Kong, X. Type synthesis of multi-mode mobile parallel mechanisms based on refined virtual chain approach. *Mech. Mach. Theory* **2020**, *152*, 103908. [CrossRef]
22. Qin, Y.; Dai, J.S.; Gogu, G. Multi-furcation in a derivative queer-square mechanism. *Mech. Mach. Theory* **2014**, *81*, 36–53. [CrossRef]
23. Kong, X. Variable degree-of-freedom spatial mechanisms composed of four circular translation joints. *ASME J. Mech. Robot.* **2021**, *13*, 031007. [CrossRef]
24. Arponen, T.; Piipponen, S.; Tuomela, J. Kinematical analysis of Wunderlich mechanism. *Mech. Mach. Theory* **2013**, *70*, 16–31. [CrossRef]
25. Wang, J.; Kong, X. A novel method for constructing multimode deployable polyhedron mechanisms using symmetric spatial compositional units. *ASME J. Mech. Robot.* **2019**, *11*, 020907. [CrossRef]
26. Tian, C.; Zhang, D.; Tang, H.; Wu, C. Structure synthesis of reconfigurable generalized parallel mechanisms with configurable platforms. *Mech. Mach. Theory* **2021**, *160*, 104281. [CrossRef]
27. Liu, R.; Li, R.; Yao, Y.-A.; Ding, X. A reconfigurable deployable spatial 8R-like mechanism consisting of four angulated elements connected by R joints. *Mech. Mach. Theory* **2023**, *179*, 105103. [CrossRef]
28. Laliberté, T.; Gosselin, C. Construction, mobility analysis and synthesis of polyhedra with articulated faces. *ASME J. Mech. Robot.* **2014**, *6*, 011007. [CrossRef]
29. Overvelde, J.; Weaver, J.; Hoberman, C.; Bertoldi, K. Rational design of reconfigurable prismatic architected materials. *Nature* **2017**, *54*, 347–352. [CrossRef] [PubMed]

30. Yan, H.; Kuo, C. Topological representations and characteristics of variable kinematic joints. *ASME J. Mech. Des.* **2006**, *128*, 384–391. [CrossRef]

31. Gan, D.; Dai, J.S.; Caldwell, D.G. Constraint-Based Limb Synthesis and Mobility-Change-Aimed Mechanism Construction. *ASME J. Mech. Des.* **2011**, *133*, 051001. [CrossRef]

32. Jia, P.; Li, D.; Zhang, Y.; Yang, C. A novel reconfigurable parallel mechanism constructed with spatial metamorphic four-link mechanism. *Proc. Inst. Mech. Eng. Part C* **2022**, *236*, 4120–4132. [CrossRef]

33. Li, Z.; Scharler, D.F.; Schröcker, H.-P. Factorization results for left polynomials in some associative real algebras: State of the art, applications, and open questions. *J. Comput. Appl. Math.* **2019**, *349* , 508–522. [CrossRef]

34. Montes, A.; Wibmer, M. Software for discussing parametric polynomial systems: The Gröbner Cover. In *Mathematical Software—ICMS 2014*; Hong, H., Yap, C., Eds.; Springer: Berlin, Germany, 2014; pp. 406–413.

35. Cox, D.A.; Little, J.B.; O'Shea, D. *Ideals, Varieties, and Algorithms*; Springer: New York, NY, USA, 2007.

36. Husty, M.L.; Schröcker, H.-P. Kinematics and algebraic geometry. In *21st Century Kinematics*; McCarthy J.M., Ed.; Springer: London, UK, 2013; pp. 85–123.

37. Wampler, C.; Sommese, A. Numerical algebraic geometry and algebraic kinematics. *Acta Numer.* **2011**, *20*, 469–567. [CrossRef]

38. Shabani, A.; Porta, J.M.; Thomas, F. A branch-and-prune method to solve closure equations in dual quaternions. *Mech. Mach. Theory* **2021**, *164*, 104424. [CrossRef]

39. Pellegrino, S. Structural computations with the singular value decomposition of the equilibrium matrix. *Int. J. Solids Struct.* **1993**, *30*, 3025–3035. [CrossRef]

40. Song, C.Y.; Chen, Y.; Chen, I.-M. A 6R linkage reconfigurable between the line-symmetric Bricard linkage and the Bennett linkage. *Mech. Mach. Theory* **2013**, *70*, 278–292. [CrossRef]

41. Wang, Y.; Zhang, Q.; Zhang, X.; Cai, J.; Jiang, C.; Xu, Y.; Feng, J. Analytical and numerical analysis of mobility and kinematic bifurcation of planar linkages. *Int. J. Non-Linear Mech.* **2022**, *145*, 104110. [CrossRef]

42. Kang, X.; Lei, H.; Li, B. Multiple bifurcated reconfiguration of double-loop metamorphic mechanisms with prismatic joints. *Mech. Mach. Theory* **2022**, *178*, 105081. [CrossRef]

43. Müller, A. Local kinematic analysis of closed-loop linkages—Mobility, singularities, and shakiness. *ASME J. Mech. Robot.* **2016**, *8*, 041013. [CrossRef]

44. Lopez-Custodio, P.C.; Rico, J.M.; Cervantes-Sanchez, J.J.; Perez-Soto, G.I.; Díez-Martínez, C.R. Verification of the higher order kinematic analyses equations. *Eur. J. Mech. A Solids* **2017**, *61*, 198–215. [CrossRef]

45. Lopez-Custodio, P.C.; Rico, J.M.; Cervantes-Sanchez, J.J. Local analysis of helicoid-helicoid intersections in reconfigurable linkages. *ASME J. Mech. Robot.* **2017**, *9*, 031008. [CrossRef]

46. Müller, A. Recursive higher-order constraints for linkages with lower kinematic pairs. *Mech. Mach. Theory* **2016**, *100*, 33–43. [CrossRef]

47. Kong, X. A novel construction method for the type synthesis of variable-DOF mechanisms. In Proceedings of the 5th IEEE/IFToMM International Conference on Reconfigurable Mechanisms and Robots, Toronto, ON, Canada, 12–14 August 2021; Xi, F., Dai, J.S., Ding, X., van der Wijk, V., Eds.; Ryerson University: Toronto, ON, Canada, 2021; pp. 31–40.

48. Kong, X. Motion/structure mode analysis and classification of n-RR planar parallelogram mechanisms. *Mech. Mach. Theory* **2022**, *169*, 104623. [CrossRef]

49. Dhingra, A.K.; Almadi, A.N.; Kohli, D. Closed-form displacement analysis of 8, 9 and 10-link mechanisms: Part I: 8-link 1-DOF mechanisms. *Mech. Mach. Theory* **2000**, *35*, 821–850. [CrossRef]

50. Qiao, S.; Liao, Q.; Wei, S.; Su, H.-J. Inverse kinematic analysis of the general 6R serial manipulators based on double quaternions. *Mech. Mach. Theory* **2010**, *45*, 193–199. [CrossRef]

51. Kiper, G.; Gürcü, F.; Korkmaz, K.; Söylemez, E. Kinematic design of a reconfigurable deployable canopy. In *New Trends in Mechanism and Machine Science*; Flores, P., Viadero, F., Eds.; Springer: Cham, Switzerland, 2015; pp. 167–174.

52. Gao, Y.; Yang, F.; Zhang, J. A reconfigurable 6R linkage with six motion modes and three topological structures. *ASME J. Mech. Robot.* **2023**, *15*, 054503. [CrossRef]